Supporting Information

Röder et al. 10.1073/pnas.0914087107

1. Carlson CR, *et al.* (2006) Delineation of type I protein kinase A-selective signaling events using an RI anchoring disruptor. *J Biol Chem* 281:21535–21545.
2. De Corte V, *et al.* (2002) Gelsolin-induced epithelial cell invasion is dependent on Ras-Rac signaling. *EMBO J* 21:6781–6790.
3. Röder IV, *et al.* (2008) Role of Myosin Va in the plasticity of the vertebrate neuromuscular junction in vivo. *PLoS One* 3:e3871.
4. Day RN (1989) Walder JA (1989) Maurer RA (1989) A protein kinase inhibitor gene reduces both basal and multihormone-stimulated prolactin gene transcription. *J Biol Chem* 264:431–436.
5. Di Benedetto G (2008) *et al.* (2008) Protein kinase A type I and type II define distinct intracellular signaling compartments. *Circ Res* 103:836–844.

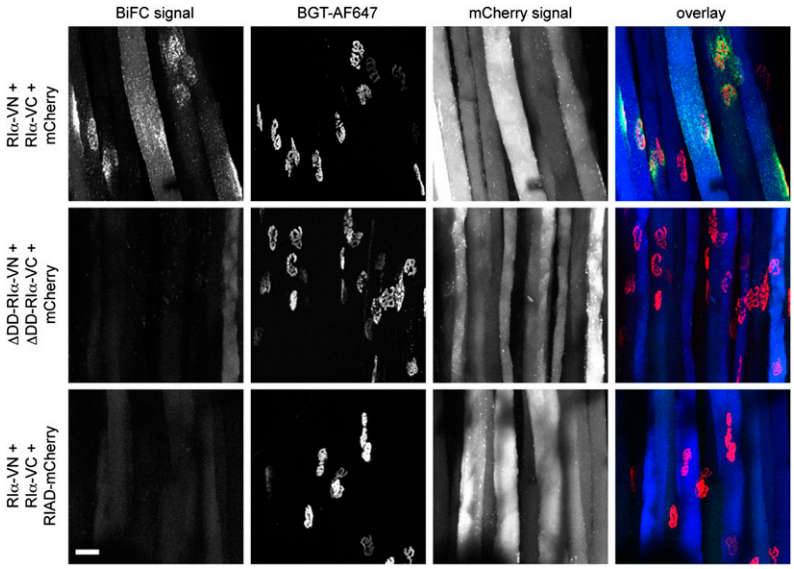

Fig. S1. Transgene protein kinase A (PKA) RIα dimerizes in a subsynaptic region in an AKAP-dependent manner in live mouse muscle. Tibialis anterior (TA) muscles were cotransfected with constructs as indicated (*Left*). For bimolecular fluorescence complementation (BiFC) constructs, human PKA RIα including (RIα) or excluding the first 62 amino acids (ΔDD-RIα) were amplified by PCR with *Nhe*I sites at 5′ and 3′ ends. These sequences were cloned into *Nhe*I-digested pBiFC-VNCT and pBiFC-VCCT. pBiFC vectors use pcDNA3.1(+) and contain HA tag sequence (YPYDVPDYA) 3′ of the *Nhe*I site followed by sequences encoding amino acids 1 to 172 (pBiFC-VNCT) or 155 to 238 (pBiFC-VCCT) of Venus. Cytoplasmic mCherry and RIAD-mCherry were expressed in pcDNA3. Ten days later muscles were injected with BGT-AF647 and monitored by in vivo confocal microscopy. Therefore, images were taken at 8-bit, 512 × 512 pixels, 200-Hz scan frequency, 2× line average. Then, 25 pmol of BGT-AF647 were injected intramuscular at least 30 min before microscopy. BiFC (excitation 514 nm, emission 519–555 nm), mCherry (excitation 561 nm, emission 580–620 nm), and AF647 signals (excitation 633 nm, emission 660–750 nm) were imaged simultaneously. (Scale bar, 50 μm.) Images depict representative three-dimensional (3D) projections of BiFC, acetylcholine receptors (BGT-AF647), mCherry fluorescence signals, and overlays (BiFC, *green*; BGT-AF647, *red*; mCherry, *blue*).

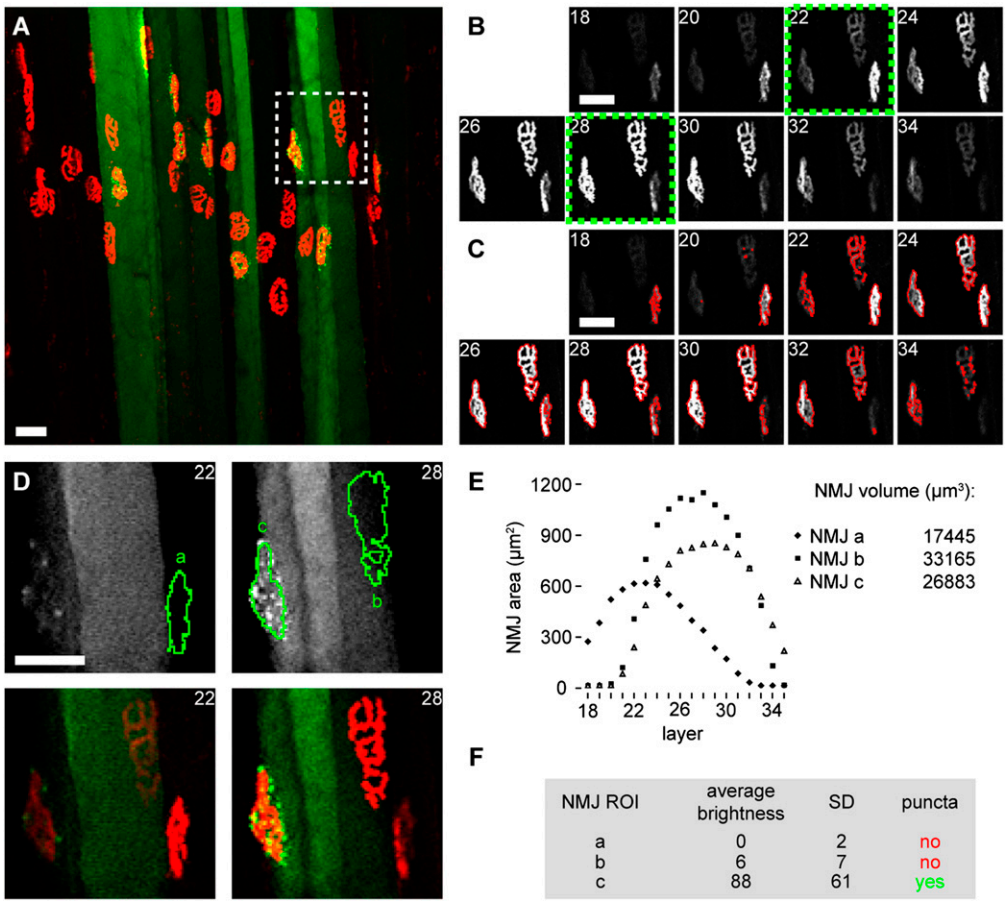

Fig. S2. Workflow for the quantitative analysis of neuromuscular junction (NMJ) size and accumulation of RIα-EPAC. The shown TA muscle was transfected with RIα-EPAC. Ten days later, it was injected with BGT-AF647 and monitored by in vivo confocal microscopy. RIα-EPAC (excitation 514 nm, emission 519–555 nm) and AF647 signals (excitation 633 nm, emission 660–750 nm) were monitored simultaneously. (Scale bars, 50 μm.) (*A*) The image shows a representative 3D projection of 45 optical sections taken at 3-μm interslice intervals. RIα-EPAC (*green*) and BGT-AF647 signals (*red*) are depicted. (*B*) Array of individual optical sections of the boxed area shown in *A* depicting BGT-AF647 signals. The confocal slice number is indicated for each image. (*C*) Same set of images as shown in *B*, but with the NMJ objects used for quantification of NMJ size outlined in red. These objects were found by thresholding the BGT-AF647 after background subtraction and applying a threshold of 70 to 255. (*D*) Images show either RIα-EPAC signals only (*Upper*) or the overlay of RIα-EPAC (*green*, *Lower*) and BGT-AF647 signals (*red*, *Lower*) for the optical sections 22 and 28 (boxed in *B*) to highlight the three possible types of NMJ: (*a*) fiber and NMJ are RIα-EPAC-negative; (*b*) fiber is RIα-EPAC-positive, but does not show accumulation of the probe in the NMJ; (*c*) fiber is RIα-EPAC-positive and shows accumulations of the probe in the NMJ. (*E*) NMJ volumes were determined by calculating the NMJ areas in each image plane multiplied with 3 μm to account for the interslice distance. The graph shows the NMJ area distribution over different optical sections of the NMJs depicted in *B*–*D*. (*Right*) Values indicate the volumes of NMJs -a, -b, and -c. (*F*) To determine, whether an NMJ exhibits accumulations of RIα-EPAC, we performed the analysis for each NMJ in the optical layer showing its largest dimension (i.e., layers 22 for NMJ-a and 28 for NMJs-b and -c, see also *E*). In these sections, three types of information were extracted within the corresponding NMJ regions (see *green* outlines a, b, and c in *D*) from the background-subtracted RIα-EPAC images: average brightness, SD, and the presence of puncta. Only fibers with an average brightness value > 1 were considered RIα-EPAC-positive; only fibers with an SD > 10 (empirically best fitting to most NMJs exhibiting clear enrichments of RIα-EPAC) were scored to potentially exhibit RIα-EPAC clusters in the NMJ; to exclude false-positives (like NMJs lying at the border between bright and dark fibers), the final criterion was the presence of punctate RIα-EPAC fluorescence signals within the outlined NMJ region. Only NMJs fulfilling all criteria were considered to exhibit RIα-EPAC accumulation in the NMJ region.

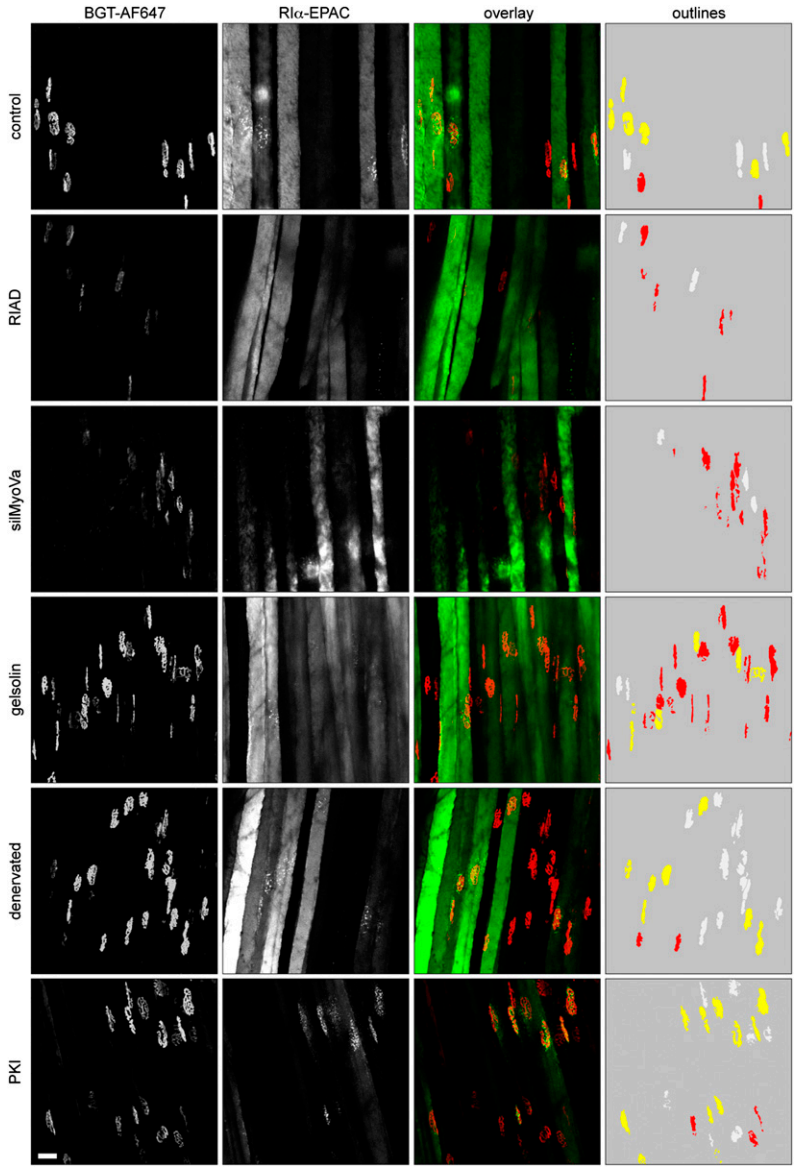

Fig. S3. Subsynaptic localization of RIα-EPAC is ablated by RI anchoring disruptor (RIAD), silMyoVa, and gelsolin, but not upon denervation and inhibition of PKA activity in vivo. TA muscles were either transfected with RIα-EPAC (control) or cotransfected with RIα-EPAC and RIAD (RIAD), silMyoVa (silMyoVa), gelsolin-GFP (gelsolin), or PKI (PKI). Some muscles were transfected with RIα-EPAC and denervated (denervated). RIAD (1) and gelsolin-GFP (2) were gifts from J. Scott (Oregon Health and Science University) and J. Gettemans (University of Ghent, Belgium). SilMyoVa (3), PKI (4), and RIα-EPAC (5) were as described. Ten days later, muscles were injected with BGT-AF647 and monitored with in vivo confocal microscopy. Shown are 3D projections of AChR staining (BGT-AF647) and RIα-EPAC, as indicated. Overlays: BGT-AF647 signals (*red*); RIα-EPAC signals (*green*). Outlines: NMJs were segmented and color-coded; (*yellow*) NMJs of RIα-EPAC-positive fibers with subsynaptic RIα-EPAC accumulations; (*red*) NMJs of RIα-EPAC-positive fibers without subsynaptic RIα-EPAC accumulations; (*gray*) NMJs of RIα-EPAC-negative fibers. (Scale bar, 50 μm.)

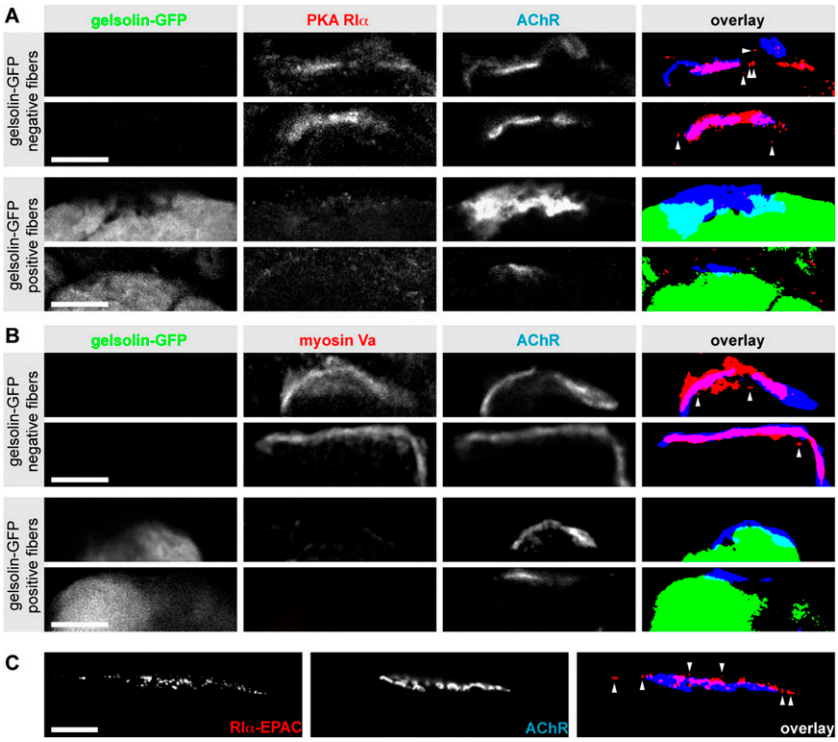

Fig. S4. Endogenous PKA RIα and myosin Va are displaced from their subsynaptic locations in the presence of gelsolin. (*A* and *B*) TA muscles were transfected with gelsolin-GFP. Ten days later, muscles were sliced transversally. For slice preparation, excised TA muscles were washed in PBS, snap-frozen and stored at −80 °C. Transversal sections were made with a Leica CM1900 cryostat and placed on electrostatic slides (Labonord). For immunostaining, slices were incubated with primary antibody over night at 4 °C. After washing, they were incubated with secondary antibody for 2 h at room temperature. Slices were washed with 10% FBS/PBS, PBS and H_2O, and embedded in Mowiol (Calbiochem). Slices were stained with BGT-AF647 (acetylcholine receptor) and immunolabeled using polyclonal primary antibodies against PKA RIα (Cell Signaling Technology) (*A*) or myosin Va (LF-18 from Sigma) (*B*) and a goat anti-rabbit-AF546 secondary antibody (Invitrogen). For confocal analysis, GFP was excited at 488 nm and emission-detected from 495 to 550 nm. AF546 and AF647 were excited at 561 nm and 633 nm, respectively. Emission was detected from 570 to 620 nm (AF546) and from 650 to 750 nm (AF647). Images were taken at 1024 × 1024 pixels. Shown are single confocal planes of gelsolin-GFP, immunostaining and BGT-AF647 (AChR) fluorescence signals, as indicated. Overlays: Fluorescence signals are binarized. Gelsolin-GFP signals (*green*); BGT-AF647 signals (*blue*); immunostaining signals (*red*); Colocalizing green and red (*yellow*); green and blue (*cyan*); red and blue (*magenta*); red, green, and blue (*white*). (*arrowheads*) Subsynaptic punctate immunostaining signals. (Scale bars, 10 μm.) (*C*) In vivo side-view of a NMJ shows a high degree of overlap between RIα-EPAC and AChR staining. A TA muscle was transfected with RIα-EPAC. Ten days later, it was injected with BGT-AF647 and monitored with in vivo confocal microscopy. Shown is a single optical slice with RIα-EPAC and AChR fluorescence signals as indicated. Overlay: Fluorescence signals are binarized. RIα-EPAC signals (*red*); BGT-AF647 signals (*blue*). Colocalizing red and blue (*magenta*). (*arrowheads*) Subsynaptic punctate RIα-EPAC fluorescence signals. (Scale bar, 10 μm.)

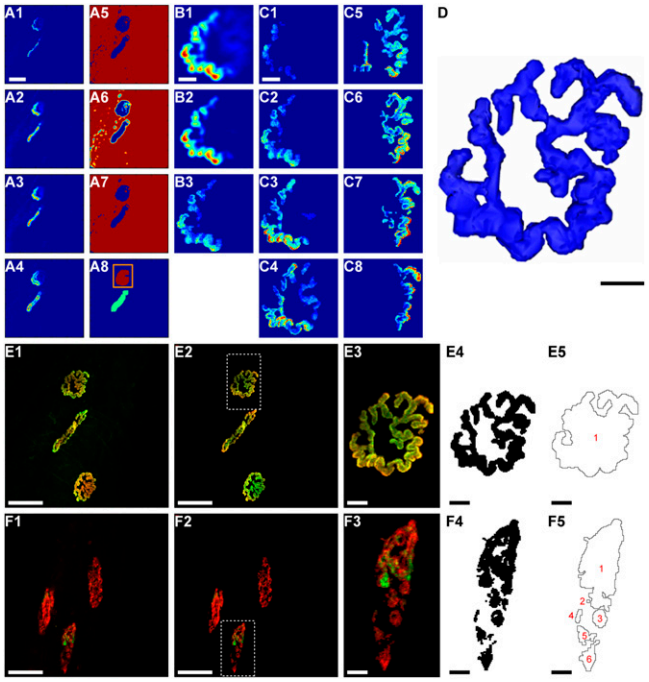

Fig. S5. Workflow for the segmentation and automated quantitative analysis of in vivo acquired NMJs. The shown TA muscles were either transfected with RIα-EPAC (*A*–*E*) or cotransfected with RIα-EPAC and silMyoVa (*F*). During transfection, muscles were injected with BGT-AF647 to stain old receptors. Ten days later, BGT-AF555 was injected to label new receptors and both were then monitored simultaneously by in vivo confocal microscopy (AF555: excitation 561 nm, emission 570–620 nm; AF647: excitation 633 nm, emission 660–750 nm). (*A*) Automated AChR-detection and quantification used MATLAB 5.3. First, pixel intensities of both channels were added to reveal sum images (*A1*). Then, a global filter extracted regions of interest (ROI) using low-pass filters (*A2*), plausibility checks (*A3*), and gradient magnitude filters (*A4*). Ninety percent of the brightest pixels were deleted and the images binarized (*A5*). Further low-pass filtering (*A6*) and thresholding (*A7*) removed artifacts. A closing routine merged small objects, an opening routine deleted small regions and a local filter extracted the position of NMJs within ROIs (*A8*). (Scale bar, 50 μm.) (*B*) Segmentation and sharpening routine for the NMJ boxed in *A8* consisting of a low-pass filter, a minimum value subtraction and an erosion routine: Original image (*B1*), first sharpening run (*B2*), second sharpening run (*B3*). (Scale bar, 10 μm.) (*C*) Example of all consecutive segmented slices comprising the NMJ boxed in *A8*. For this type of experiment, confocal sections were taken every 1.5 μm. (Scale bar, 10 μm.) (*D*) 3D-structures of NMJs were obtained by comparison of detected 2D-NMJs in the 3D-sequence of images. The image depicts an automatically detected 3D view of the NMJ boxed in *A8*. (Scale bar, 10 μm.) For the quantification of old-receptor and new-receptor intensities, all 2D-objects belonging to a NMJ were labeled. Then, relative intensities of old-receptor and new-receptor signals were extracted and calculated to quantify 3D-NMJs. (*E* and *F*) Images show a comparison of original (*E1* and *F1*) and automatically segmented data (*E2* and *F2*) as well as the mode of quantification of fragments of the NMJs boxed in *E2* and *F2* (*E3*–*E5* and *F3*–*F5*). *E1* to *E3* and *F1* to *F3* show 3D projections of the overlay of old receptors (*green*) and new receptors (*red*). Pixels with similar intensity in both channels appear yellow. *E4* and *F4* show binarized images used for the scoring of fragments per NMJ. *F4* and *F5* depict the identified fragments with numbering (one fragment in *E*, six fragments in *F*). [Scale bars, 50 μm (*E1* and *E2*, *F1* and *F2*) or 10 μm (*E3*–E5, *F3*–*F5*).]

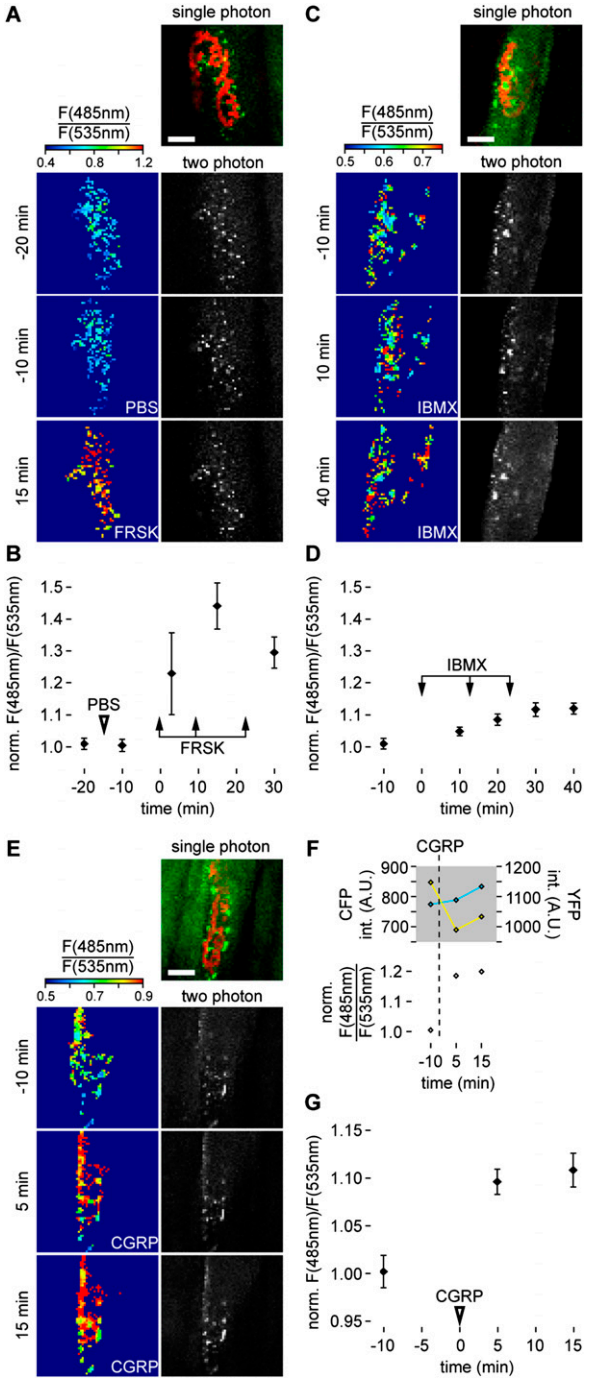

Fig. S6. Characterization of cAMP measurements in the NMJ region using the RIα-EPAC probe. TA muscles were transfected with RIα-EPAC. Ten days later, they were injected with BGT-AF647 and then monitored by in vivo confocal microscopy or two-photon microscopy (indicated). For two-photon microscopy, RIα-EPAC was excited with a Maitai laser at 810 nm. CFP and YFP signals were simultaneously detected by nondescanned detectors using RSP 505 dichroic mirror and BP485/30 and BP560/50 emission filters (Leica). Photomultiplier gains and offsets were kept constant, laser intensity was adjusted according to sample depth. Images were taken at 12-bit, 512 × 512 pixel, 200-Hz scan frequency, 2× line average. The following drugs (all from Sigma, PBS from Invitrogen) were injected in a volume of 50 μL intramuscular with a 30× gauge syringe as indicated: PBS (*A* and *B*), 100 μM forskolin (FRSK, *A* and *B*), 500 μM IBMX (*C* and *D*), or 10 μM CGRP (*E*–*G*). Final agonist concentrations were presumably much lower in the muscle fibers analyzed because of distribution of the solution in the muscle volume and drain off by blood circulation. For recovery from injection-induced swelling microscopy was paused for 2 min after injection. Imaging in the presence of the agonists usually started 3 to 5 min after drug application. (*A*, *C*, and *E*) Representative images of cAMP measurement experiments. (*Top*) Single optical plane with the overlay of RIα-EPAC (*green*) and BGT-AF647 signals (*red*). (Scale bars, 10 μm.) (*Lower Right*) Single optical planes of two-photon YFP images of the same field of view at different time points before and after drug application (indicated on the *Left*). (*Lower Left*) Pseudo color-coded CFP/YFP ratio-images of the frames shown on the right. The color bar above each ratio-image column indicates the pseudo color corresponding to a given CFP/YFP ratio value. (*B*, *D*, and *G*) Graphs show the mean CFP/YFP ratio values of all measured NMJs ± SEM (data normalized to basal value; $n = 13$ NMJs in *B*, $n = 11$ NMJs in *D*, and $n = 41$ NMJs in *G*) as a function of time after drug injection obtained from at least three different experiments. For data analysis, the following protocol was employed: Upon background subtraction, a CFP/YFP ratio-image stack was made. Coarse identification of sensor-positive subsynaptic regions was done by correlating accumulations of RIα-EPAC signals in the two-photon images with BGT-AF647 signals in the single photon images. Then, pixels above fiber background level were identified in two-photon YFP images. Corresponding ROIs before and after stimulus application were determined in 10 subsequent

Legend continued on following page

optical sections. CFP/YFP ratio values were read out in these ROIs in corresponding ratio-image stacks. The time-points of drug injection are indicated by an arrowhead (PBS in *B*, CGRP in *G*) or by arrows (FRSK in *B*, IBMX in *D*). The time point of the first injection of FRSK, IBMX, or CGRP was set as time 0. (*F*) Individual traces of CFP (*cyan*) and YFP (*yellow*) and corresponding CFP/YFP ratio values normalized to the basal value of the NMJ depicted in *E*. CGRP was injected at zero minutes.

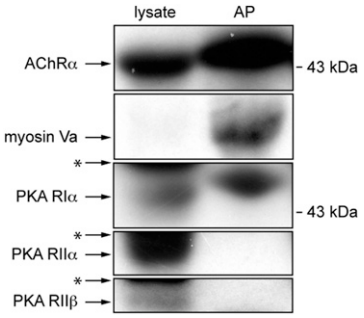

Fig. S7. Myosin Va and PKA RIα coprecipitate with surface-exposed or endocytosed/recycling AChR. Wild-type mice were injected in vivo with BGT-biotin. Then, TA muscles were sampled from killed animals and lysates were prepared. Subsequently, lysates were incubated with NeutrAvidin beads and acetylcholine receptors were affinity precipitated. Bands show Western blot signals from lysates and affinity precipitates (AP) using antibodies against proteins as indicated. Asterisks indicate nonspecific bands. Primary antibodies were monoclonal anti-AChRα, anti-PKA RIα, anti-PKA RIIα, and anti-PKA RIIβ (all BD Bioscience), as well as polyclonal anti-myosin Va (LF-18, Sigma). Secondary antibodies were anti-mouse-HRP and anti-rabbit-HRP (Dako). For protocol, see Röder et al. [Röder IV, et al. (2008) Role of Myosin Va in the plasticity of the vertebrate neuromuscular junction in vivo. *PLoS One*. 3:e3871.].

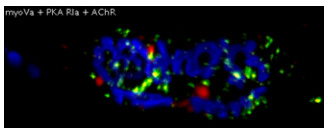

Movie S1. Three-dimensional localization of markers for PKA RIα, myosin Va, and AChR in vivo. TA muscles were cotransfected with RIα-EPAC and MCST-DsRed (from H. Gerdes, University of Bergen, Norway). Ten days later, the muscles were injected with BGT-AF647 and imaged with in vivo confocal microscopy. The movie shows a representative 3D projection of 20 optical planes taken with 1.5-μm interslice interval, rotating two times by 360°. Depicted are fluorescence signals of the markers for PKA RIα (*green*), myosin Va (*red*), and AChR (*blue*). During the first turn, the green channel was omitted for better visibility of the other signals. The last image shows the approximate fiber outline (*dotted line*).

Movie S1